Journal of the Brazilian Society of Mechanical Sciences and Engineering (2022) 44:198
https://doi.org/10.1007/s40430-022-03396-z

TECHNICAL PAPER

# A study on the electroosmotic flow of micropolar fluid in a channel with hydrophobic walls

Fateme Karampour[1] · Amin Haghighi Poshtiri[1] · Amin Hadizade[1]

Received: 9 August 2021 / Accepted: 28 January 2022 / Published online: 22 April 2022


## Abstract
In the present study, the equations governing the electroosmotic flow in a horizontal microchannel with hydrophobic walls are solved using the micropolar fluid model analytically. The effects of the influential parameters, including micropolar viscosity, the ratio of characteristic length of the fluid microstructures to the characteristic length of the flow ($m$), concentration coefficient, Debye–Hückel parameter, the ratio of pressure-driven velocity to electroosmotic velocity ($U_r$), and slip coefficient, were examined on the flow pattern. According to the results, the magnitude of the velocity profile decreases as the micropolar viscosity, $m$, and $U_r$ ($U_r < 0$) increase. The flow velocity grows as the concentration coefficient-dependent microgyration flow distribution increases, and the velocity distribution increases as the $U_r$ ($U_r > 0$) and Debye–Hückel parameter acting as the flow's electric driving force. The slip coefficient has a direct impact on the velocity profile, considerably increasing its value. Thus, it can be concluded that small-scale surface slip is highly significant and helps achieve the best design of microchannel walls to control the flow in microchannels accurately. In addition, the contrast between decreasing velocity profile and increasing micropolar viscosity makes the micropolar fluid model an appropriate tool to simulate the fluid behavior in microstructures, given that it assumes gyration in the boundaries due to the existence of an electric field.

**Keywords** Electroosmotic flow · Micropolar fluid · Hydrophobic wall

### List of symbols

| | |
|---|---|
| $b$ | Slip coefficient |
| $e$(C) | Charge of an electron |
| $E$ ($V$ m$^{-1}$) | Applied electric field |
| $h$ (m) | Height of the microchannel |
| $j_0$ (m$^2$) | Microinertia parameter |
| $k_B$ | Boltzmann constant ($1.38 \times 10^{-23}$ J K$^{-1}$) |
| $L$(m) | Length of the microchannel |
| $m_0$ | Dimensionless Debye–Hückel parameter |
| $n$ | Concentration coefficient |
| $n_0$ (m$^{-3}$) | Bulk concentration of ions |
| $N$ | Dimensionless gyration component |
| $p$ (kg m$^{-1}$ s$^{-2}$) | Fluid pressure |
| $P$ | Dimensionless pressure |
| $s$, $w$ | Couple stress parameters |
| $T$ (K) | Absolute temperature |
| $U$ | Dimensionless velocity component |
| $U_e$ (m s$^{-1}$) | The characteristic velocity of an electric field |
| $U_p$ (m s$^{-1}$) | Pressure-driven flow velocity |
| $v$ (s$^{-1}$) | Microgyration velocity component |
| $V$ (m s$^{-1}$) | Fluid velocity component |
| $x$, $y$ | Dimensionless Cartesian coordinates |
| $z$ | Valence of ions |

### Dimensionless Number

| | |
|---|---|
| $Re$ | Reynolds number |
| $Ro$ | Microgyration Reynolds number |
| $m$ | The ratio of characteristic length of the fluid microstructures to the characteristic length of the flow |

Technical Editor: Ahmad Arabkoohsar.

This article has been selected for a Topical Issue of this journal on Nanoparticles and Passive-Enhancement Methods in Energy.

✉ Amin Haghighi Poshtiri
Haghighi_p@guilan.ac.ir

Fateme Karampour
Fatemekarampour76@gmail.com

Amin Hadizade
Aminhadi1371@gmail.com

[1] Faculty of Mechanical Engineering, University of Guilan, P.O. Box 3756, Rasht, Iran

| | |
|---|---|
| $K$ | Dimensionless micropolar viscosity |
| $U_r$ | The ratio of pressure-driven velocity to electroosmotic velocity |

**Greek symbols**

| | |
|---|---|
| $\chi$ (kg m$^{-1}$s$^{-1}$) | Rotational viscosity coefficient |
| $\mu$ (kg m$^{-1}$s$^{-1}$) | Dynamic viscosity coefficient |
| $\alpha, \beta, \gamma$ (kg m s$^{-1}$) | Angular viscosity coefficients |
| $\alpha_0$ | Ionic energy parameter |
| $\rho$ (kg m$^{-3}$) | Density of fluid |
| $\varphi$ (V) | Total electric potential |
| $\phi$ (V) | External electric potential |
| $\psi$ (V) | EDL potential |
| $\lambda_D$ (m) | Debye length |
| $\psi_0$ (V) | Zeta potential |
| $\epsilon$ (C V$^{-1}$ m$^{-1}$) | Permittivity of the solution |
| $\rho_e$ (C m$^{-3}$) | Net electric charge density |

## 1 Introduction

Given the great advances in the technologies for fabricating devices and systems on micro and nanoscales, especially electromechanical systems, electroosmotic micropumps are an efficient solution for fluid transport within microfluidic systems due to their numerous advantages, especially having no moving parts [1].

Electroosmosis is known as a major phenomenon in electrokinetic transport. This phenomenon was discovered in 1809 by Reuss [2], who observed the motion of water during the transport of an external electric field. Subsequently, numerous researchers showed interest in investigating this subject. Smoluchowski [3] was the first to propose an analytical solution for the electroosmotic flow (EOF) in a simple channel. In a study in 1998, Patankar and Hu [4] presented a finite volume-based numerical scheme to simulate EOFs in complex geometries. So far, extensive research has been performed on electrokinetic transport phenomena classified according to different factors, such as fluid type, microchannel type, and flow analysis type, examining the effects of various parameters, such as Joule heating, electric double-layer (EDL) potential, and external pressure gradient, on the heat transfer and flow behavior. Furthermore, different methods have been introduced for flow analysis. In a numerical study, Park et al. [5] investigated the EOF inside various microchannels using the Nernst–Planck and the Poisson–Boltzmann methods. They stated that in problems with small EDL thicknesses, the difference between the two models was very small. Moreover, the Poisson–Boltzmann model was more efficient in simple geometries and for modeling internal electric potential. However, the Nernst–Planck model was more suitable for complex geometries due to the significance of ion displacement and concentration. Over recent years, non-Newtonian fluids have received special attention due to their important engineering and industrial applications. However, given the diversity of the fundamental equations in these fluids and the fact that the Navier–Stokes equations cannot accurately represent the properties of Newtonian fluids, which do not contain suspended particles, micropolar models can be effective in better describing the behavior of Newtonian and non-Newtonian fluids. In 1965, Eringen [6] formulated the micropolar fluid theory for the first time to describe fluid behavior on a small scale.

The results of this study are practicable and can be helpful for the development of technologies such as capillary electrochromatography (CEC) [7].

### 1.1 Electroosmotic flow of a micropolar fluid

Investigations into the EOF of the micropolar fluids have indicated that considering the role of suspended particles in the fluid, along with the micropolar theory, plays a key role in understanding the pattern of flows subject to magnetic and electric fields, such as EOFs, especially in microstructures [8–12]. A review of the literature is performed as follows to gain a better understanding of this subject.

Misra et al. [13] conducted a semi-analytical study on the micropolar fluid flow in a microchannel under the effect of a variable electric field. They simulated blood flow between two plates with an infinite depth as a case of bio-microfluidics with micropolar properties. Their results indicated that changing the micropolarity of the fluid and the height between the two plates led to a change in the flow velocity, and using the nonzero boundary condition for the microgyrations altered the thickness of the EDL. Ding et al. [14] presented an analytical solution for the time-varying EOF of an incompressible micropolar fluid inside parallel microchannels. They realized that with an increase in the micropolarity of the fluid, the velocity range and the volumetric flow rate decreased to near zero. The results also showed that the electric potential effect on the micropolar fluid was similar to that on the Newtonian fluid. However, it could cause a difference in the microgyrations. Chaube et al. [15] conducted an analytical study on the peristaltic flows of biological micropolar fluids via the electroosmosis mechanism using a parallel plate microchannel. The results showed that the peristaltic pumping of a micropolar fluid escalated with the use of an external electric field and changed with the formation of an EDL. It was observed that since the flows were in one direction, the streamlines were trapped near the EDL, becoming parallel in the middle of the microchannel. However, when the EOF was not along the peristaltic flow, the flow was trapped in the middle of the microchannel.

In the most recent research on the EOF of a micropolar fluid, Tripathi et al. [16] carried out a numerical study considering the effects of double-diffusive convection heat transfer for a micropolar fluid flow created by a peristaltic pump and the electroosmotic mechanism inside an asymmetric microchannel. They showed that the Helmholtz–Smoluchowski velocity considerably affected the fluid particles' velocity, pressure gradient, and microgyration in tolerating the velocity slip, the buoyancy effect, and the EDL phenomenon. In addition, the temperature of the nano-fluid rose with the thermal diffusivity and the Prandtl number. Saleem et al. [17] proposed a comprehensive mathematical model to analyze the peristaltic flow of a Bingham viscoplastic micropolar fluid inside a wavy microchannel with an electroosmotic actuator. They stated that the electroosmotic effects mostly assisted the flow control, and higher electric field strengths resulted in lower axial velocity and higher microgyration velocity.

A disadvantage of microchannels is the large pressure drop along them compared to channels with conventional dimensions. Hence, using hydrophobic surfaces as a factor that reduces pressure drop is recommended. Hydrophobic surfaces repel water. This phenomenon is due to the unbalance between the molecular forces at the water–solid interface, which causes surface tension [18]. The behavior of water droplets on a surface can be associated with two factors: surface energy and wettability. When a material has larger energy on the surface, the surface is hydrophilic, and thus, a smaller contact angle is created. On the other hand, if the surface energy of a material is small, the molecules in the water droplets are more attracted to each other than to the surface, hence creating a larger contact angle and a hydrophobic surface. Moreover, wettability is the capability of a liquid in contact with a solid surface and results from intermolecular forces [19]. One of the most practical methods of creating a hydrophobic surface is using polymer composites that give hydrophobic properties to the textures surface and bond it to the substrate, thereby stabilizing the hydrophobic walls [18]. In addition, slip velocity and temperature jump are two factors affecting the heat transfer and pressure drop in hydrophobic surfaces [20]. The following reviews some of the previous research in this field.

### 1.2 Electroosmotic flow with hydrophobic surfaces

Soong et al. [21] performed an analysis of electrokinetic flows subject to pressure in a one-dimensional hydrophobic microchannel considering the effects of slip and slip-dependent zeta potential on Newtonian fluids. Their results showed that the slip effects were effective only in small length ranges, and the super-hydrophobicity of the channel walls was not effective in increasing the flow and saving pumping power. Sadeghi et al. [22] analyzed the fully developed EOF in hydrophobic microchannels with different cross sections with the Debye–Hückel approximation using the Navier slip condition. They demonstrated that the flow velocity increased linearly with the slip length for a thin EDL. Silkina et al. [23] proposed a theory for flat and cylindrical nano-channels containing hydrophobic surfaces. Their theory consisted of the movement of the attracted surface charges and hydrodynamic slip for describing EOFs. They also showed that the EDL and fluid slip near the hydrophobic surface affected the hydrodynamic diffusivity of the nano-structures. Rahmati et al. [24] presented a model using the lattice Boltzmann method to calculate the slip length in EOFs on hydrophobic walls. Their results indicated that slipping on the channel boundaries extended the flow development time, and slipping on the walls prevented lateral changes in the velocity profile while causing a significant quantitative increase, improving the performance of the electroosmotic pump. Noreen et al. [25] studied the effects of slippage and Joule heating in EOF through peristalsis in an asymmetric microchannel to investigate the entropy generation in a magnetohydrodynamic non-Newtonian Jeffery fluid flow numerically. They concluded that the axial velocity of the EOF in the Jeffrey fluid was higher than that of the Newtonian fluids, and the velocity generation increased in porous media and with parameters, such as the electroosmotic parameter and the zeta potential at the upper wall. However, the slip length and zeta potential at the lower wall reduced velocity production for a porous medium, and the Joule heating increased entropy generation.

In a recent study, Baños et al. [26] numerically examined the effects of rheology and slippage of non-Newtonian fluids on the mass transport of species due to an oscillatory electroosmotic flow using a power-law model. The results showed that by considering the slippage, more suitable conditions could be created for mass transport of species for different values of Schmidt number and a Womersley number of less than one.

To the best of knowledge of the authors of this study, the effect of slippage on electroosmotic flow of micropolar fluids has never been considered in other investigations. Micropolar fluid theory has proven to have higher accuracy in explaining fluid behavior in microscale in the presence of potential field. This innate quality gives this model a priority to be utilized in relevant physics, Therefore, this study has analytically investigated the effect of the influential parameters, including micropolar viscosity ($K$), the ratio of characteristic length of the fluid microstructures to the characteristic length of the flow ($m$), concentration coefficient ($n$), Debye–Hückel parameter ($m_0$), the ratio of pressure-driven velocity to electroosmotic velocity ($U_r$), and slip coefficient ($b$), on the flow behavior by examining the velocity and gyration profiles.

## 2 Problem geometry

Figure 1 shows a symbolic design of an EOF in a microchannel with hydrophobic walls. The basic equations governing an incompressible, axially symmetric micropolar fluid, ignoring the volumetric forces and gravity, are as follows [8]:

$$\nabla^{*}.\boldsymbol{V}^{*} = 0 \tag{1}$$

$$-(\mu+\chi)\nabla^{*}\times\left[\nabla^{*}\times\boldsymbol{V}^{*}\right]+\chi\nabla^{*}\times\boldsymbol{v}^{*}+\rho_{e}^{*}\boldsymbol{E}-\nabla^{*}.\boldsymbol{P}^{*}=\rho\left[\boldsymbol{V}^{*}.\nabla^{*}\right]\boldsymbol{V}^{*} \tag{2}$$

$$(\alpha+\beta+\gamma)\nabla^{*}\left[\nabla^{*}.\boldsymbol{v}^{*}\right]-\gamma\nabla^{*}\times\left[\nabla^{*}\times\boldsymbol{v}^{*}\right] \\ -2\chi\boldsymbol{v}^{*}+\chi\nabla^{*}\times\boldsymbol{V}^{*}=\rho j_{0}\left[\boldsymbol{V}^{*}.\nabla^{*}\right]\boldsymbol{v}^{*} \tag{3}$$

The expressions $\boldsymbol{V}$ and $\boldsymbol{v}$ are the fluid velocity and microgyration, respectively, $\boldsymbol{E}$ is the applied electric field, $\boldsymbol{P}$ is the fluid pressure, and $\rho$ and $j_0$ denote mass density and microinertia, respectively. Moreover, $\alpha$, $\beta$, and $\gamma$ are angular viscosity coefficients, and μ and χ are the dynamic and rotational viscosity coefficients, respectively.

## 3 Electric field equations

According to Fig. 1, the EOF is caused by creating a dual zone and applying the internal electric field in the vicinity of the charged walls of the channel. In order to calculate the velocity field, first, the distribution of the electric potential obtained through the Poisson equation is defined as follows:

$$\nabla^{2}\psi(y)=-\frac{\rho_{e}}{\epsilon} \tag{4}$$

where $\rho_e$ is the electric charge density and $\epsilon$ is the permittivity of the solution. For small Debye lengths and zeta potentials, the electric potential can be considered the sum of the potential derived from the EDL ($\psi$) and the potential caused by the external electric field ($\phi$) [27].

$$\varphi=(\phi+\psi) \tag{5}$$

By assuming that the electrolyte solution is symmetrical, Boltzmann distribution can be used for charge density within the electrolyte solution:

$$\rho_{e}=ze\left(n^{+}-n^{-}\right)=-2n_{0}ze\sinh\left(\frac{ze\psi}{k_{B}T}\right) \tag{6}$$

In the above equation, $z$ represents valence of ions, $e$ is the electron charge, $n_0$ is the desired ion concentration, $k_B$ is the Boltzmann constant, and $T$ denotes the absolute temperature in kelvin.

The Debye length is also much smaller than the height of the microchannel ($h>>\lambda_D$) [8]:

$$\lambda_{D}=\sqrt{\frac{\epsilon k_{B}T}{2n_{0}(ze)^{2}}} \tag{7}$$

The characteristic velocity of an electric field can be defined as follows [8]:

$$U_{e}=-\frac{\epsilon\psi_{0}E_{0}}{\mu} \tag{8}$$

in which $E_0=|\boldsymbol{E}|\geq 0$ and $\psi_0$ is called zeta potential.

For an incompressible micropolar fluid, the continuity, momentum, and microgyration equations are defined using the dimensionless form as follows [8]:

$$\nabla.\boldsymbol{V}=0 \tag{9}$$

$$-\nabla\times[\nabla\times\boldsymbol{V}]+K\nabla\times\boldsymbol{v}+\rho_{e}\boldsymbol{E}/E_{0}=\nabla\cdot\boldsymbol{P}+Re[\boldsymbol{V}.\nabla]\boldsymbol{V} \tag{10}$$

$$-\nabla\times[\nabla\times\boldsymbol{V}]-2s\boldsymbol{v}+w\nabla[\nabla.\boldsymbol{v}]+s\nabla\times\boldsymbol{V}=Ro[\boldsymbol{V}.\nabla]\boldsymbol{v} \tag{11}$$

where $K$ represents the micropolar viscosity, $s$ and $w$ are the couple stress parameters, $Re$ denotes the Reynolds number, and $Ro$ represents the microgyration Reynolds number.

According to Ref. [28], $s$ equals $\frac{10K}{m^{2}(1+\frac{K}{2})}$, in which $m$ indicates the ratio of characteristic length of the fluid microstructures to the characteristic length of the flow and varies between 0.1 and 1.

Based on the theory of electric field, the governing equation for the distribution of electrostatic potential in the Poisson equation is defined by substituting Eq. (6) in Eq. (4) as follows:

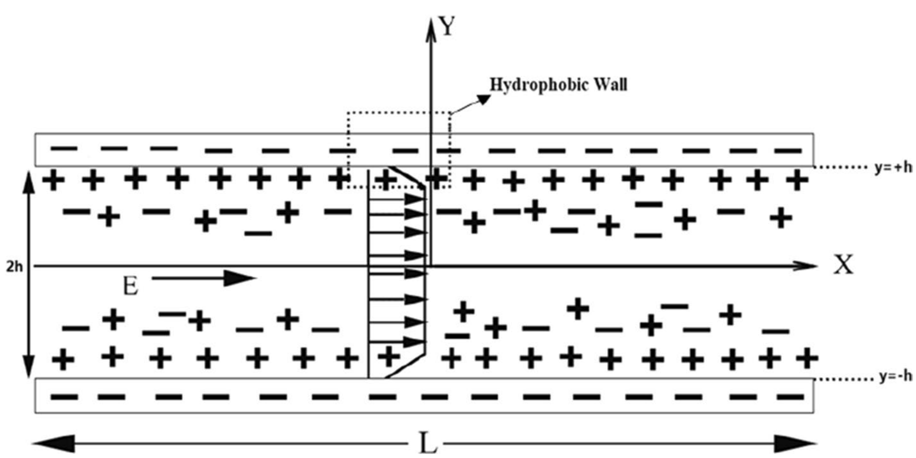


**Fig. 1** Symbolic design of problem geometry and flow

$$\nabla^2\psi(y) = \frac{m_0^2}{\alpha_0}\sinh\left[\alpha_0\psi(y)\right] \tag{12}$$

and a group of dimensionless parameters is defined as follows:

$$\begin{aligned}
&K = \chi/\mu \quad s = \chi h^2/\gamma \quad w = (\alpha+\beta+\gamma)/\gamma \\
&Re = \rho U_e h/\mu \quad P = \left(p - p_0\right)/(\tfrac{1}{2}\rho U_e^2) \quad U_r = U_p/U_e \\
&U_p = -h^2(dp/dx)/\mu \quad Ro = \rho j_0 U_e h/\gamma \quad m_0 = h/\lambda_D \\
&\alpha_0 = ze\psi_0/k_B T
\end{aligned} \tag{13}$$

The symbols $U_p$, $U_r$, $m_0$, and $\alpha_0$ denote the pressure-driven flow velocity, the ratio of pressure-driven velocity to electroosmotic velocity, the Debye–Hückel parameter, and the ionic energy parameter, respectively.

By using the Taylor expansion, the hyperbolic sine function in Eq. (12) can be linearized:

$$\nabla^2\psi(y) = m_0^2\psi(y) \tag{14}$$

By solving the above general differential equation, Eq. (14) can be solved as follows:

$$\psi(y) = \frac{\cosh\left(m_0 y\right)}{\cosh\left(m_0\right)} \tag{15}$$

Herein, the changes along the $x$-axis are ignored. Concerning the $y$-axis, the one-dimensional flow is smooth and symmetrical.

According to the definitions presented, Eqs. (9)–(11) provide the following two differential equations:

$$U''(y) + \frac{K}{K+1}N'(y) + \frac{1}{K+1}\psi''(y) + \frac{U_r}{K+1} = 0 \tag{16}$$

$$N''(y) - sU'(y) - 2sN(y) = 0 \tag{17}$$

By integrating Eq. (16) and using Eq. (15), Eq. (18) is obtained as follows:

$$U'(y) = -\frac{K}{K+1}N(y) - \frac{m_0\sinh\left(m_0 y\right)}{(K+1)\cosh\left(m_0\right)} - \frac{U_r}{K+1}y \tag{18}$$

Since the flow is symmetrical, we have:

$$U'(0) = 0, \psi'(0) = 0 \tag{19}$$

The boundary conditions intended for $U(y)$ and $\psi(y)$ are as follows:

$$U(\pm 1) = 0, \psi(\pm 1) = 0 \tag{20}$$

By substituting Eq. (18) in Eq. (17), we have:

$$N''(y) - \left(2s - \frac{sK}{K+1}\right)N(y) + \frac{sm_0\sinh\left(m_0 y\right)}{(K+1)\cosh\left(m_0\right)} + \frac{sU_r}{K+1}y = 0 \tag{21}$$

By using the D-operator, the solution of the above equation is obtained as follows:

$$\begin{aligned}
N(y) = {} & ae^{\sqrt{\left(2s-\frac{sK}{K+1}\right)}y} + be^{-\sqrt{\left(2s-\frac{sK}{K+1}\right)}y} \\
& + \frac{s}{\left(2s - \frac{sK}{K+1}\right)(K+1)}U_r y \\
& + \frac{\frac{sm_0}{(K+1)\cosh\left(m_0\right)}}{\left(2s - \frac{sK}{K+1}\right) - m_0^2}\sinh\left(m_0 y\right)
\end{aligned} \tag{22}$$

The following provides the boundary conditions for the gyration on walls:

$$N(\pm 1) = -n\frac{dU}{dy}|_{y=\pm 1} \tag{23}$$

in which $n$ is the microgyration boundary parameter (concentration coefficient). As for boundary conditions, various arguments provide analytical and numerical results in Ref. [8] for zero as well as nonzero, and if:

$$N(0) = 0 \rightarrow a + b = 0 \tag{24}$$

the general solution of Eq. (22) is considered a coefficient like $c$ whose value is calculated:

$$\begin{aligned}
N(y) = {} & c\sinh\left(\sqrt{\left(2s - \frac{sK}{K+1}\right)}y\right) \\
& + \frac{s}{\left(2s - \frac{sK}{K+1}\right)(K+1)}U_r y \\
& + \frac{\frac{sm_0}{(K+1)\cosh\left(m_0\right)}}{\left(2s - \frac{sK}{K+1}\right) - m_0^2}\sinh\left(m_0 y\right)
\end{aligned} \tag{25}$$

By using boundary conditions (24) in the above equation, the coefficient $c$ is obtained:

$$\begin{aligned}
N(y) = {} & \left[\frac{\frac{-\frac{sm_0}{(K+1)\cosh\left(m_0\right)}}{\left(2s-\frac{sK}{K+1}\right)-m_0^2}\sinh\left(m_0\right) + \frac{\frac{nm_0\sinh\left(m_0\right)}{(K+1)\cosh\left(m_0\right)} + \frac{nU_r}{K+1}}{1-\frac{Kn}{1+K}} - \frac{sU_r}{\left(2s-\frac{sK}{K+1}\right)(K+1)}}{\sinh\left(\sqrt{\left(2s - \frac{sK}{K+1}\right)}\right)}\right] \\
& \sinh\left(\sqrt{\left(2s - \frac{sK}{K+1}\right)}y\right) \\
& + \frac{sU_r}{\left(2s - \frac{sK}{K+1}\right)(K+1)}y + \frac{\frac{sm_0}{(K+1)\cosh\left(m_0\right)}}{\left(2s - \frac{sK}{K+1}\right) - m_0^2}\sinh\left(m_0 y\right)
\end{aligned} \tag{26}$$

Then, equation $U(y)$ could be solved by integrating Eq. (18) and considering the Navier slip boundary conditions on walls for hydrophobic walls. Therefore:

$$
\begin{aligned}
U(y) = {} & \frac{-K\left[\dfrac{\dfrac{-\frac{sm_0}{(K+1)\cosh(m_0)}}{\left(2s-\frac{sK}{K+1}\right)-m_0^2}\sinh(m_0)+\dfrac{\frac{nm_0\sinh(m_0)}{(K+1)\cosh(m_0)}+\frac{nU_r}{K+1}}{1-\frac{Kn}{1+K}}-\dfrac{sU_r}{\left(2s-\frac{sK}{K+1}\right)(K+1)}}{\sinh\left(\sqrt{\left(2s-\frac{sK}{K+1}\right)}\right)}\right]}{(1+K)\sqrt{\left(2s-\frac{sK}{K+1}\right)}} \\
& \left[\cosh\left(\sqrt{\left(2s-\frac{sK}{K+1}\right)}y\right)-\cosh\left(\sqrt{\left(2s-\frac{sK}{K+1}\right)}\right)\right]-\left(\frac{U_r}{2(K+1)}+\frac{KsU_r}{2(K+1)^2\left(2s-\frac{sK}{K+1}\right)}\right)\left(\left(y^2-1\right)\right) \\
& -\left(\frac{\frac{Ksm_0}{(K+1)\cosh(m_0)}}{m_0(1+K)\left(\left(2s-\frac{sK}{K+1}\right)-m_0^2\right)}\right)\left[\cosh(m_0y)-\cosh(m_0)\right]-\left(\frac{1}{K+1}\right)\left[\frac{\cosh(m_0y)}{\cosh(m_0)}-1\right] \\
& -b\left[-\frac{K}{K+1}\left[\left[\frac{\dfrac{-\frac{sm_0}{(K+1)\cosh(m_0)}}{\left(2s-\frac{sK}{K+1}\right)-m_0^2}\sinh(m_0)+\dfrac{\frac{nm_0\sinh(m_0)}{(K+1)\cosh(m_0)}+\frac{nU_r}{K+1}}{1-\frac{Kn}{1+K}}-\dfrac{sU_r}{\left(2s-\frac{sK}{K+1}\right)(K+1)}}{\sinh\left(\sqrt{\left(2s-\frac{sK}{K+1}\right)}\right)}\right]\right.\right. \\
& \left.\left.\sinh\left(\sqrt{\left(2s-\frac{sK}{K+1}\right)}\right)+\frac{sU_r}{\left(2s-\frac{sK}{K+1}\right)(K+1)}+\frac{\frac{sm_0}{(K+1)\cosh(m_0)}}{\left(2s-\frac{sK}{K+1}\right)-m_0^2}\sinh(m_0)\right]-\frac{m_0\sinh(m_0)}{(K+1)\cosh(m_0)}-\frac{U_r}{K+1}\right]
\end{aligned}
\tag{27}
$$

In the above equation, $b$ indicates the slip coefficient of the surfaces.

Accordingly, Eqs. (26) and (27) form the boundary value solution for the steady-state flow of a micropolar fluid when the Debye–Hückel approximation is established [8].

## 4 Validation of the solution

The analytical solutions were validated with two different cases. First, the velocity profile of the flow with the electroosmotic/pressure actuator for different values of $U_r$ was compared with the analytical solution of the electroosmotic/pressure-driven flow in a straight two-dimensional channel [29]. Then, the velocity distribution of the micropolar fluid at various $K$s was compared to the analytical results of [30], which were presented for the Poiseuille flow of micropolar fluids. A very good agreement was obtained between the results (Figs. 2, 3).

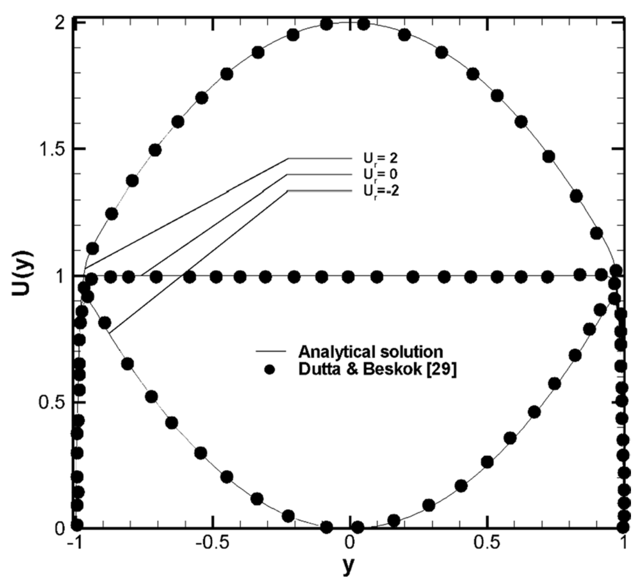


**Fig. 2** A comparison between the results of the present study and Ref. [29] to validate the velocity profiles with electroosmotic/pressure actuator for different values of $U_r$

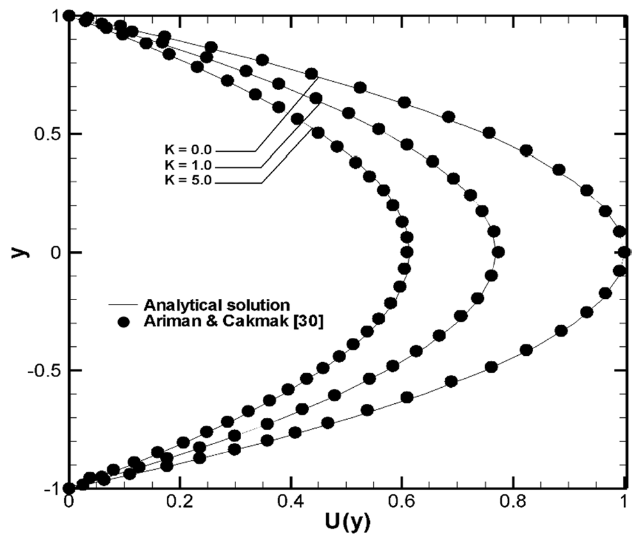


**Fig. 3** A comparison between the results of the present study and Ref. [30] to validate the velocity profiles of micropolar fluid for different values of $K$

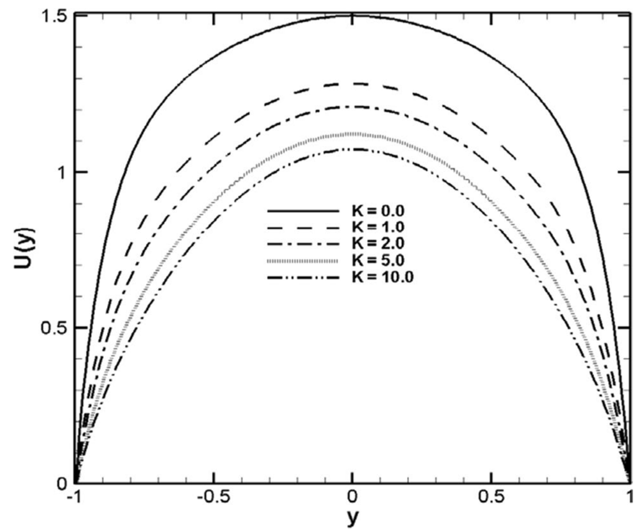


**Fig. 4** Velocity profile with electroosmotic/pressure actuator of micropolar fluid flow for different values of $K$ at $m_0=10$, $n=0.1$, $m=0.2$, $U_r=1$, $b=0$

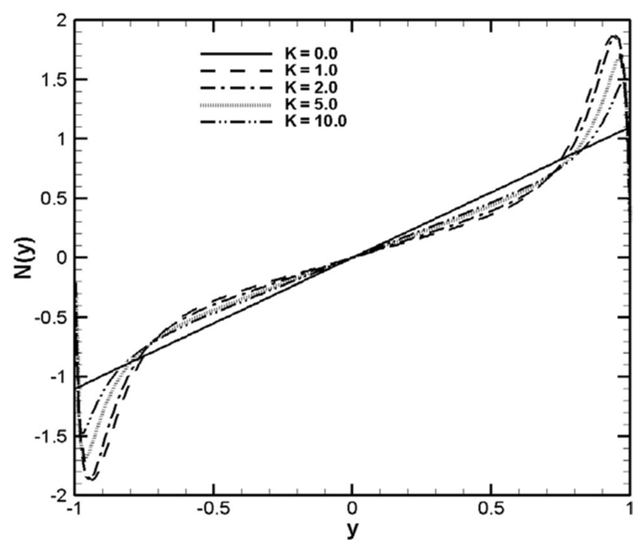


**Fig. 5** Gyration profile with electroosmotic/pressure actuator of micropolar fluid flow for different values of $K$ at $m_0=10$, $n=0.1$, $m=0.2$, $U_r=1$

## 5 Results and discussion

In this section, the results of the analytical solution are investigated, and the effect of the influential parameters, including micropolar viscosity, the ratio of characteristic length of the fluid microstructures to the characteristic length of the flow, concentration coefficient, Debye–Hückel parameter, the ratio of pressure-driven velocity to electroosmotic velocity, and slip coefficient, on the flow pattern are investigated. The following provides the distribution of velocities for the cases with the slip coefficients of 0, 0.05, and 0.1 for slippage walls, respectively.

### 5.1 Electrokinetic effects of micropolar fluids without slip

Figures 4 and 5 display the flow velocity and gyration profiles with an electroosmotic/pressure actuator in a micropolar fluid for different values of $K$ in the range of 0–10. It is observed that with an increase in the micropolar viscosity, the velocity and gyration profiles experience a reduction in magnitude. Furthermore, when $K$ equals zero, such behavior is qualitatively similar to that of Newtonian fluids.

Figures 6 and 7 depict different concentration coefficients ranging from 0 to 1, versus velocity and gyration profiles with the electroosmotic/pressure actuator in a micropolar fluid. As can be seen, at $n=0$, the fluid elements at the boundaries have no gyration. Hence, no movement is added to the flow in the microchannel given the gyration of fluid elements at the boundaries. Moreover, the magnitude of the velocity and gyration profiles has an increasing trend with the rise in $n$.

Figures 8 and 9 make a comparison between the flow velocity and gyration profiles for different values of the Debye–Hückel parameter in the range of 5–100, which is the main actuation factor of the flow. It is observed that higher values of this parameter lead to higher flow velocity and lower curvature of the velocity profile. This means a reduction in the thickness of the EDL. Moreover, given the definition of $m_0$, which is in the form of $\frac{h}{\lambda_D}$, $\lambda_D$ becomes smaller

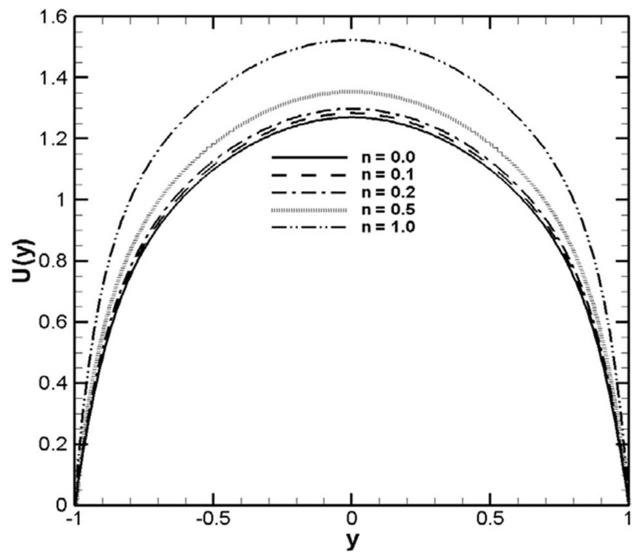


**Fig. 6** Velocity profile with electroosmotic/pressure actuator of micropolar fluid flow for different values of $n$ at $m_0=10$, $K=1$, $m=0.2$, $U_r=1$, $b=0$

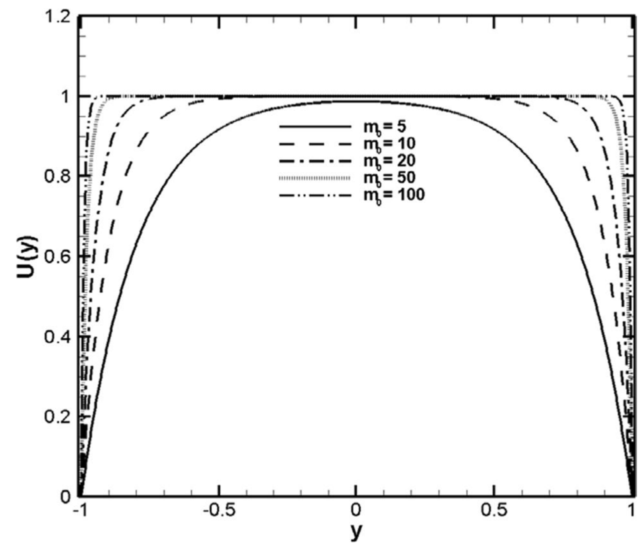


**Fig. 8** Velocity profile with pure electroosmotic actuator of micropolar fluid flow for different values of $m_0$ at $K=0$, $n=0.1$, $m=0.2$, $U_r=0$, $b=0$

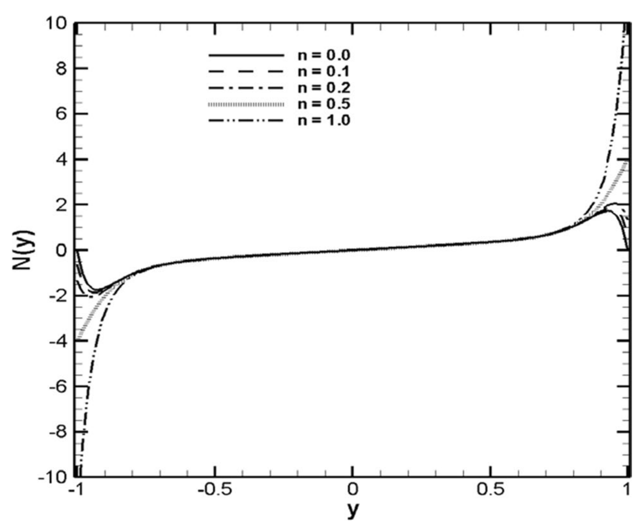


**Fig. 7** Gyration profile with electroosmotic/pressure actuator of micropolar fluid flow for different values of $n$ at at $m_0=10$, $K=1$, $m=0.2$, $U_r=1$

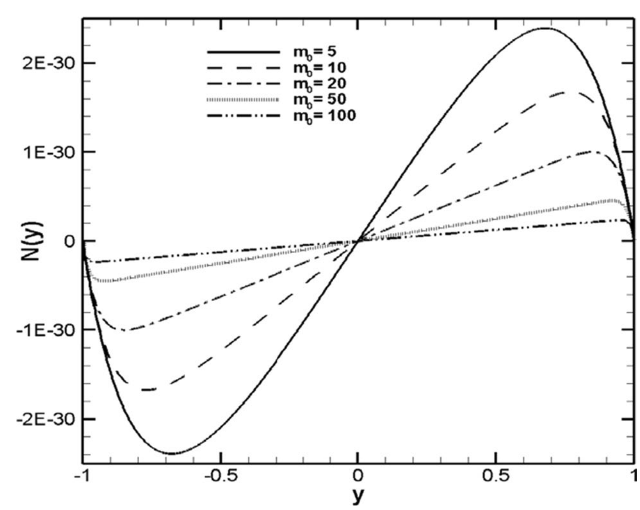


**Fig. 9** Gyration profile with pure electroosmotic actuator of micropolar fluid flow for different values of $m_0$ at at $K=0$, $n=0.1$, $m=0.2$, $U_r=0$

than $h$, and the velocity distribution tends to a constant value.

Figures 10 and 11 demonstrate the velocity and gyration profiles of the micropolar fluid for different values of $U_r$ (representing the ratio of pressure-driven velocity to electroosmotic velocity that the zeta potential can create in the flow via $m_0$) with its value ranging from -2 to 2. $U_r>0$ means that the velocity field due to electroosmotic and pressure forces is applied in the direction of the flow, and the velocity distribution rises with the pressure. On the other hand, if $U_r<0$, the velocity field is opposite to the direction of the flow, and the velocity distribution decreases. Moreover, it can be said that a zero value for this ratio means the absence of a pressure force in the flow, i.e., the fluid flow in the channel is totally driven by the electroosmotic actuator.

In Figs. 12 and 13, the velocity and gyration profiles with an electroosmotic actuator in the micropolar fluid versus the channel width can be compared for different values of $m$ ranging from 0.1 to 1. According to the figures, an increase in this parameter reduces the flow velocity. In addition, considering the concept of $m$, which represents the ratio of characteristic length of the fluid microstructures to the

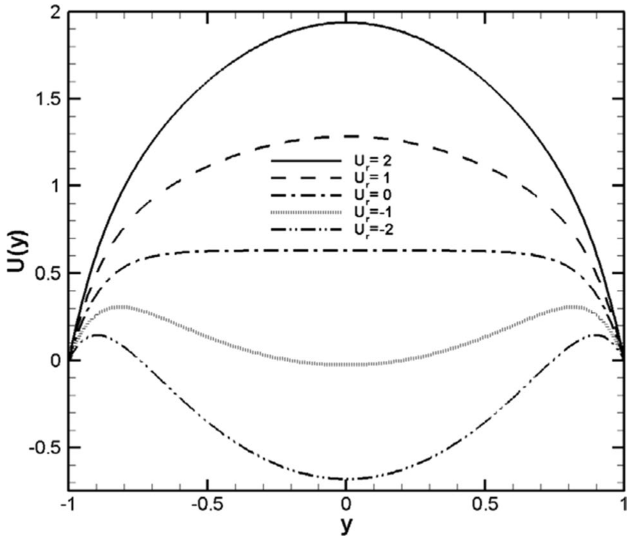


**Fig. 10** Velocity profile with electroosmotic/pressure actuator of micropolar fluid flow for different values of $U_r$ at $K=1$, $m_0=10$, $n=0.1$, m=0.2, $b=0$

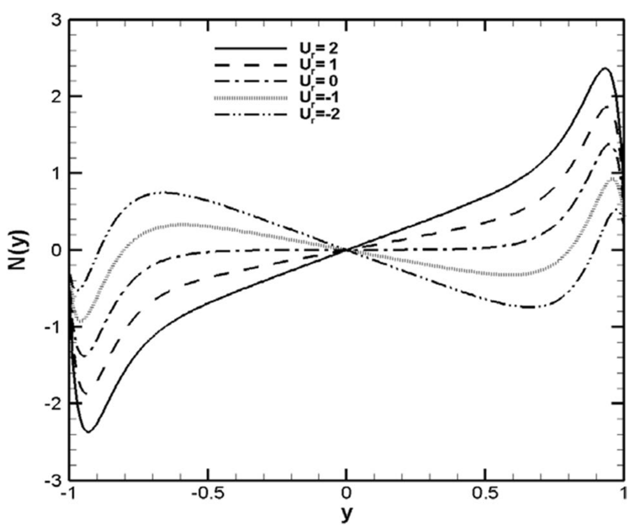


**Fig. 11** Gyration profile with electroosmotic/pressure actuator of micropolar fluid flow for different values of $U_r$ at $K=1$, $m_0=10$, $n=0.1$, $m=0.2$

characteristic length of the flow, one can infer that the flow faces lower frictional resistance at lower ratios.

Figure 14 indicates the effect of the slip coefficient in the range of 0–0.2 on the flow velocity with the electroosmotic/pressure actuator. As can be seen, as the slip coefficient rises, the resistive force of the fluid decreases, and the fluid exits the wall, increasing the flow velocity near the wall. It can be said that if a hydrophobic wall is used, the flow velocity

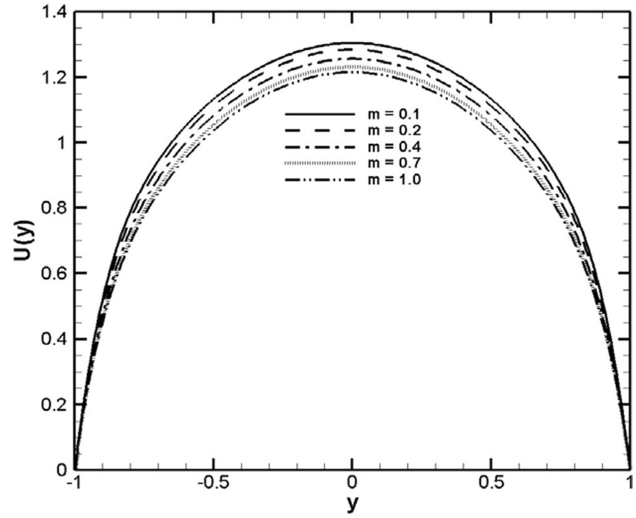


**Fig. 12** Velocity profile with electroosmotic/pressure actuator of micropolar fluid flow for different values of $m$ at $K=1$, $m_0=10$, $n=0.1$, $U_r=1$, $b=0$

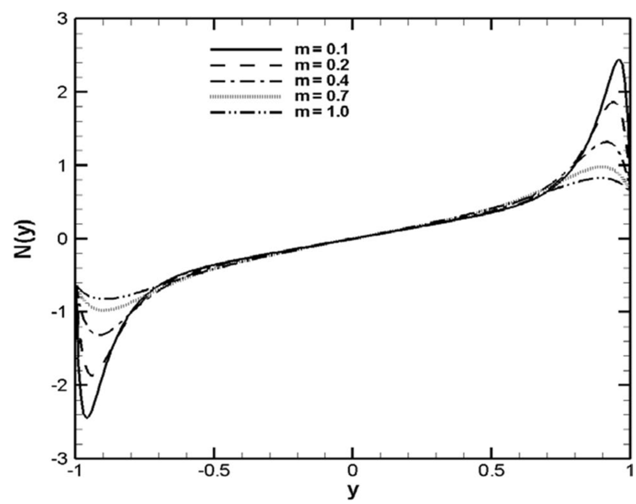


**Fig. 13** Gyration profile with electroosmotic/pressure actuator of micropolar fluid flow for different values of $m$ at $K=1$, $m_0=10$, $n=0.1$, $U_r=1$

on the wall is no longer zero. Accordingly, the slip length significantly affects the flow profile and increases its value.

## 5.2 Electrokinetic effect of micropolar fluids in the presence of slip

The following resents the EOF velocity results in the presence of surface slip.

Figures 15 and 16 indicate the velocity profiles with the electroosmotic/pressure actuator in a micropolar fluid for different values of $K$ considering wall slip. It was observed

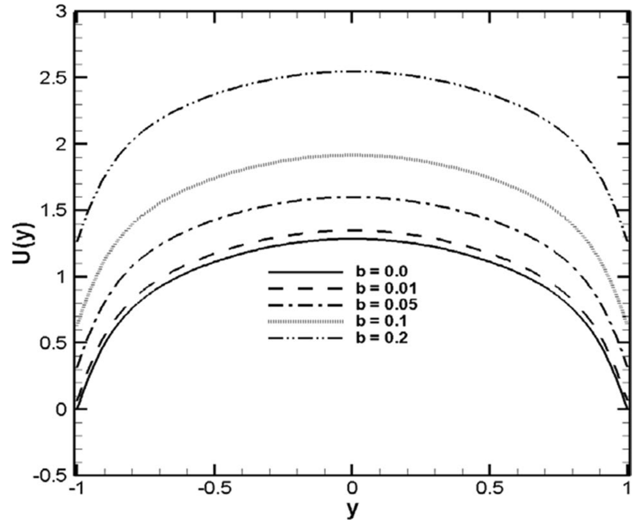


**Fig. 14** Velocity profile with electroosmotic/pressure actuator of micropolar fluid flow for different values of $b$ at $K=1$, $m_0=10$, $n=0.1$, $m=0.2$, $U_r=1$

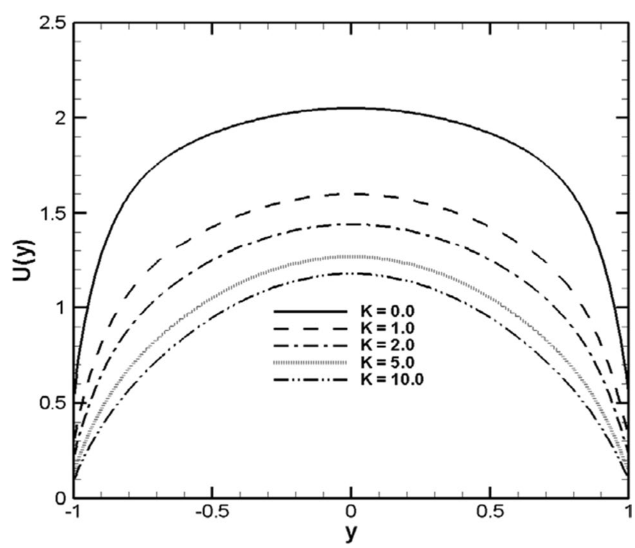


**Fig. 15** Velocity profile with electroosmotic/pressure actuator of micropolar fluid flow for different values of $K$ at $m_0=10$, $n=0.1$, $m=0.2$, $U_r=1$, $b=0.05$

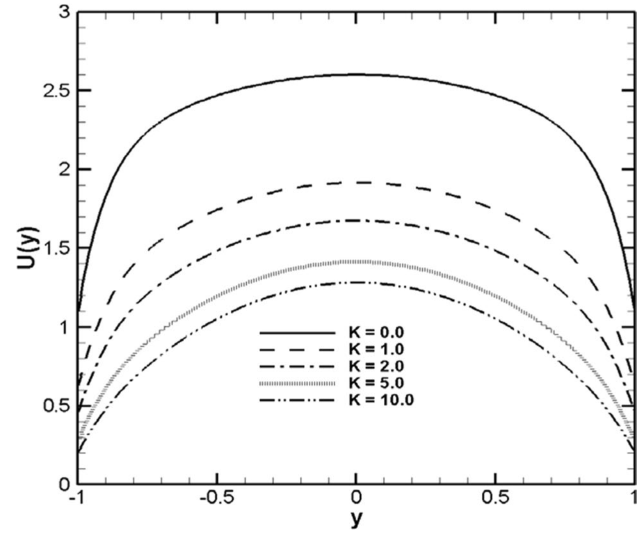


**Fig. 16** Velocity profile with electroosmotic/pressure actuator of micropolar fluid flow for different values of $K$ at $m_0=10$, $n=0.1$, $m=0.2$, $U_r=1$, $b=0.1$

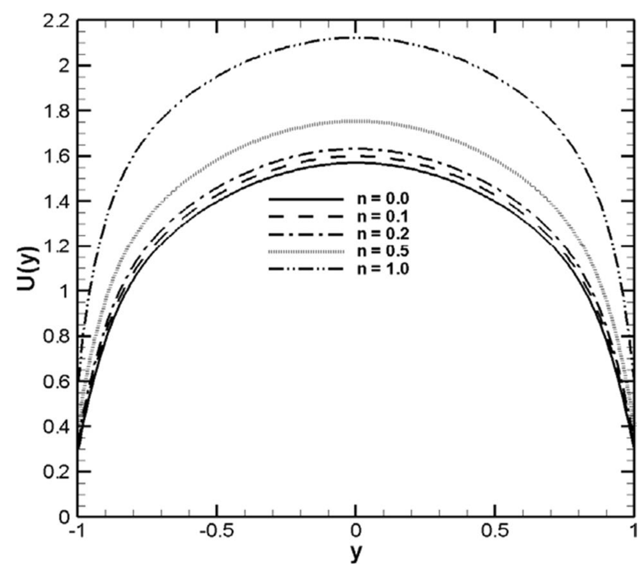


**Fig. 17** Velocity profile with electroosmotic/pressure actuator of micropolar fluid flow for different values of $n$ at $m_0=10$, $K=1$, $m=0.2$, $U_r=1$, $b=0.05$

that the decreasing trend of the velocity profile decelerates as the micropolar viscosity and slip coefficient increase.

Figures 17 and 18 illustrate different concentration coefficients for velocity profiles in a micropolar fluid with the electroosmotic/pressure actuator in the presence of wall slip. As can be seen, with a rise in the concentration and wall slip, the velocity profile extends compared to the state without slip.

Figures 19 and 20 make a comparison of the velocity profiles with hydrophobic walls for different values of the Debye–Hückel parameter. The results indicate that the velocity distribution is significantly extended in the presence of slip. Moreover, the curvature of the velocity profile is decreased, i.e., the thickness of the EDL is decreased.

Figures 21 and 22 show the velocity profiles of the micropolar fluid for different values of $U_r$ with wall slip. As mentioned previously, at $U_r > 0$, the velocity distribution increases with the pressure drive. In contrast, if $U_r < 0$, the velocity distribution declines, and the presence of a

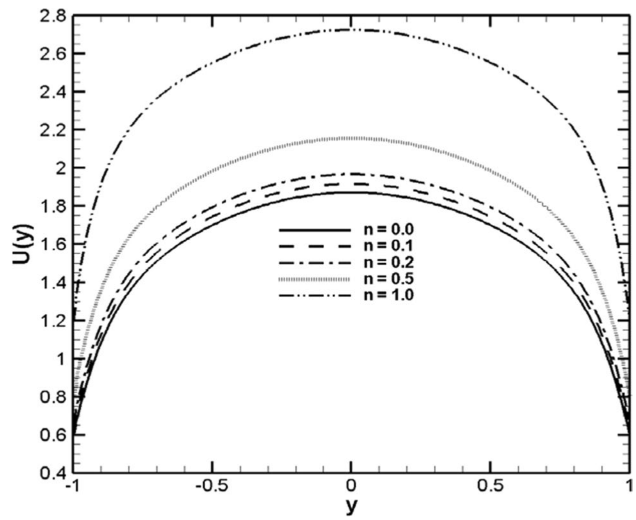


**Fig. 18** Velocity profile with electroosmotic/pressure actuator of micropolar fluid flow for different values of $n$ at $m_0=10$, $K=1$, $m=0.2$, $U_r=1$, $b=0.1$

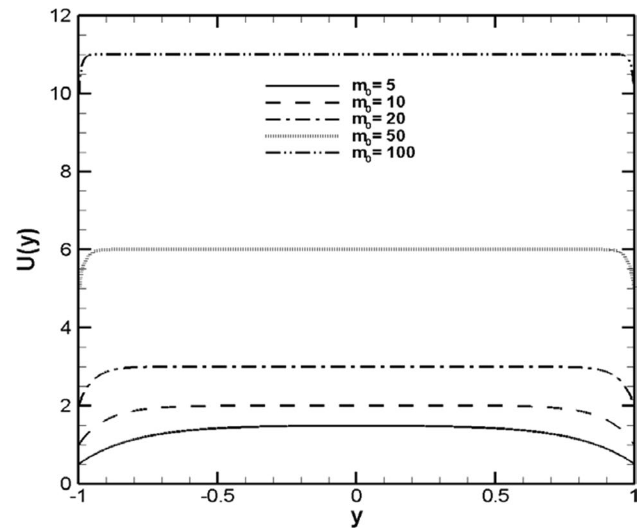


**Fig. 20** Velocity profile with pure electroosmotic actuator of micropolar fluid flow for different values of $m_0$ at $K=0$, $n=0.1$, $m=0.2$, $U_r=0$, $b=0.1$

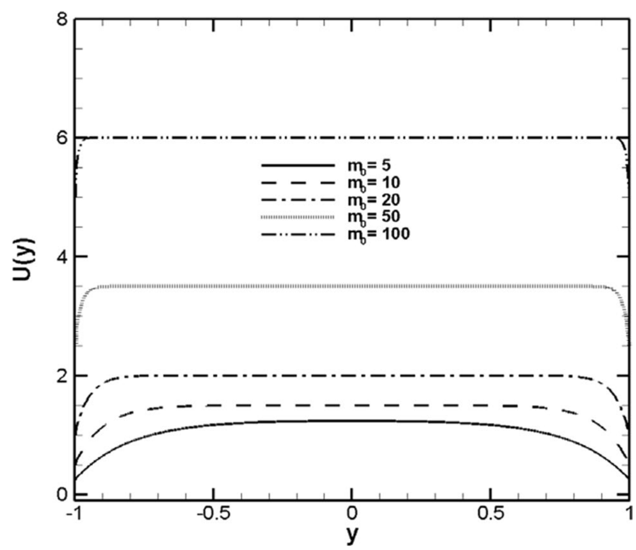


**Fig. 19** Velocity profile with pure electroosmotic actuator of micropolar fluid flow for different values of $m_0$ at $K=0$, $n=0.1$, $m=0.2$, $U_r=0$, $b=0.05$

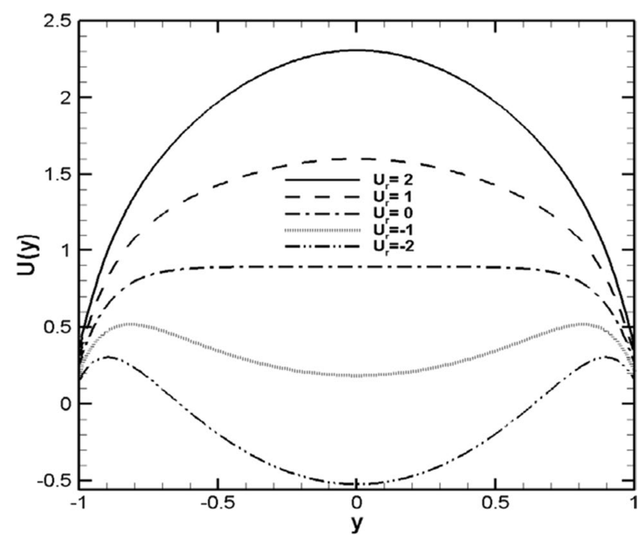


**Fig. 21** Velocity profile with electroosmotic/pressure actuator of micropolar fluid flow for different values of $U_r$ at $K=1$, $m_0=10$, $n=0.1$, $m=0.2$, $b=0.05$

hydrophobic wall significantly magnifies the effect of this parameter on the flow velocity distribution.

In Figs. 23 and 24, the velocity profiles of the micropolar fluid with the electroosmotic actuator can be compared for different values of $m$ considering wall slip. It is observed that an increase in this parameter in the presence of the slip effect decelerates the decreasing trend in the flow velocity.

## 6 Conclusions

The electroosmotic flow of a micropolar fluid model in a horizontal microchannel with hydrophobic walls is investigated analytically in this study. The findings were divided into two sections to examine the effects of the problem variables including micropolar viscosity ($K$), the ratio of characteristic length of the fluid microstructures to the

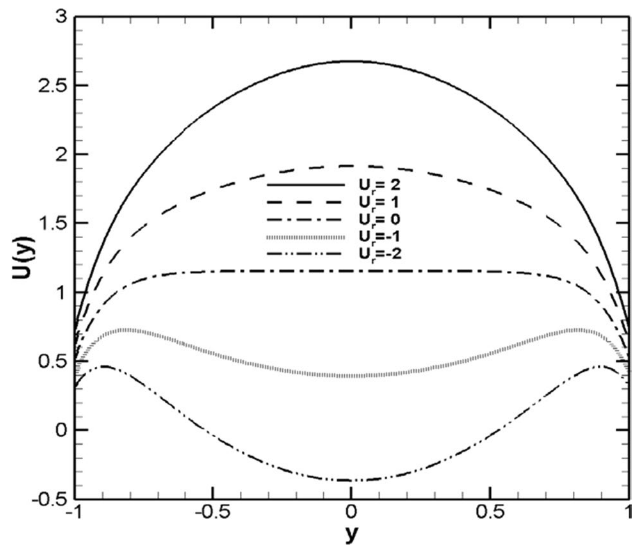


**Fig. 22** Velocity profile with electroosmotic/pressure actuator of micropolar fluid flow for different values of $U_r$ at $K=1$, $m_0=10$, $n=0.1$, $m=0.2$, $b=0.1$

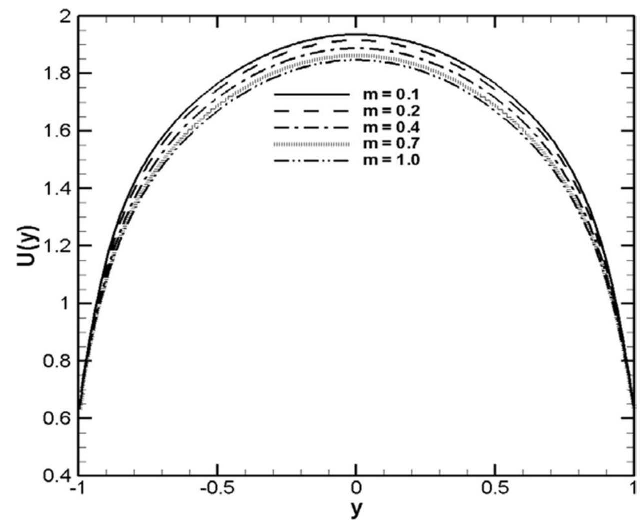


**Fig. 24** Velocity profile with electroosmotic/pressure actuator of micropolar fluid flow for different values of $m$ at $K=1$, $m_0=10$, $n=0.1$, $U_r=1$, $b=0.1$

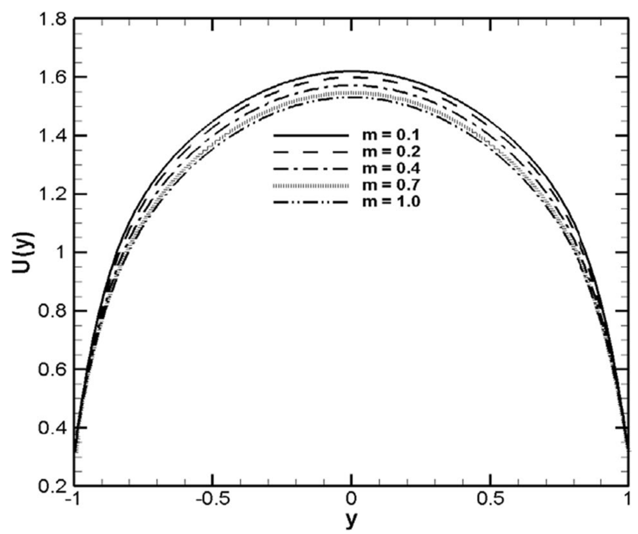


**Fig. 23** Velocity profile with electroosmotic/pressure actuator of micropolar fluid flow for different values of $m$ at $K=1$, $m_0=10$, $n=0.1$, $U_r=1$, $b=0.05$

characteristic length of the flow ($m$), concentration coefficient ($n$), Debye–Hückel parameter ($m_0$), the ratio of pressure-driven velocity to electroosmotic velocity ($U_r$), and slip coefficient ($b$). The first section examined the effect of these variables on velocity and gyration profiles without considering wall slip, and the second section examined the effect of these variables with wall slip.

The results indicated that increasing the $K$, $m$, and $U_r$ ($U_r<0$) parameters decreased the microchannel's velocity. With an increased $U_r$ ($U_r>0$), $n$ and $m_0$ parameters, the velocity inside the microchannel increased. Additionally, increasing the $m_0$ results in a reduction in the thickness of the EDL. The slip coefficient directly affects the velocity profile, significantly increasing its value. It was observed that when the wall slip is considered, the trend toward increasing the flow velocity increases as the $U_r$ ($U_r>0$), $n$, and $m_0$ parameters are increased. At the same time, the decreasing trend of the velocity distribution declines by increasing the $K$, $m$, and $U_r$ ($U_r<0$) parameters and slip coefficient. Thus, increasing the slip coefficient on the wall results in an increase in the wall's velocity.

The present analysis indicates that slip boundary condition on a small scale is highly significant and helps achieve the best microchannel walls design for accurate control of flow in microchannels. The future studies would be focused on the effects of heat transfer within the present physics by different boundary conditions and the addition of nanoparticles.

## References


1. Wang X, Wang S, Gendhar B, Cheng C, Byun CK, Li G, Zaho M, Liu S (2009) Electroosmotic pumps for microflow analysis. Trends Anal Chem 28(1):64–74
2. Reuss FF (1809) Charge-induced flow. Proc Imperial Soc Naturalists Moscow 3:327–344
3. Smoluchowski M (1903) Contribution à la théorie de l'endosmose électrique et de quelques phénomènes corrélatifs. Bulletin de l'Académie des Sciences de Cracovie 8:182–200
4. Patankar NA, Hu HH (1998) Numerical simulation of electroosmotic flow. Anal Chem 70(9):1870–1881

5. Park HM, Lee JS, Kim TW (2007) Comparison of the Nernst-Planck model and the Poisson-Boltzmann model for electroosmotic flows in microchannels. J Colloid Interface Sci 315(2):731–739
6. Eringen AC (1966) Theory of micropolar fluids. J Appl Math Mech 16(1):1–18
7. Sawada H, Jinno K (1999) Preparation of capillary columns coated with linear polymer containing hydrophobic and charged groups for capillary electrochromatography. Electrophoresis 20(1):24–30
8. Siddiqui AA, Lakhtakia A (2009) Steady electroosmotic flow of a micropolar fluid in a microchannel. Proc Roy Soc A 465:501–522
9. Mukhopadhyay A, Banerjee S, Gupta Ch (2009) Fully developed hydrodynamic and thermal transport in combined pressure and electrokinetically driven flow in a microchannel with asymmetric boundary conditions. Int J Heat Mass Transf 52(7–8):2145–2154
10. Alloui Z, Vasseur P (2010) Natural convection in a shallow cavity filled with a micropolar fluid. Int J Heat Mass Transf 53(13–14):2750–2759
11. Haghighi EA, Jafarmadar S, Khalil Arya Sh, Rezazadeh G (2017) Study of micropolar fluid flow inside a magnetohydrodynamic micropump. J Braz Soc Mech Sci Eng 39(59–66):4955–4963
12. Javed T, Mehmood Z, Siddiqui MA (2017) Mixed convection in a triangular cavity permeated with micropolar nanofluid-saturated porous medium under the impact of MHD. J Braz Soc Mech Sci Eng 39(10):3897–3909
13. Misra JC, Chandra S, Herwig H (2015) Flow of a micropolar fluid in a microchannel under the action of an alternating electric field: Estimates of flow in bio-fluidic devices. J Hydrodyn B 27(3):350–358
14. Ding Z, Jian Y, Yang L (2016) Time periodic electroosmotic flow of micropolar fluids through microparallel channel. Appl Math Mech 37(6):769–786
15. Chaube MK, Yadav A, Tripathi D, Bég OA (2018) Electroosmotic flow of biorheological micropolar fluids through microfluidic channels. Korea-Aust Rheol J 30(2):89–98
16. Tripathi D, Prakash J, Reddy MG, Misra JC (2020) Numerical simulation of double difusive convection and electroosmosis during peristaltic transport of a micropolar nanofluid on an asymmetric microchannel. J Therm Anal Calorim 143(3):2499–2514
17. Saleem A, Kiani MN, Nadeem S, Akhtar S, Ghalambaz M, Issakhov A (2021) Electroosmotically driven flow of micropolar bingham viscoplastic fluid in a wavy microchannel: application of computational biology stomach anatomy. Computer Methods Biomech Biomed Eng 24(3):289–298
18. Boinovich LB, Emelyanenko AM (2008) Hydrophobic materials and coatings: principles of design, properties and applications. Russ Chem Rev 77(7):583–600
19. Chieng BW, Ibrahim NA, Daud NA, Talib ZA (2019) Functionalization of graphene oxide via Gamma-Ray irradiation for hydrophobic materials. In: Synthesis, technology and applications of carbon nanomaterials. Elsevier, Vienna, pp 177–203
20. Roy P, Anand NK, Banerjee D (2013) Liquid slip and heat transfer in rotating rectangular microchannels. Int J Heat Mass Transf 62:184–199
21. Soong CY, Hwang PW, Wang JC (2009) Analysis of pressure-driven electrokinetic flows in hydrophobic microchannels with slip-dependent zeta potential. Microfluid Nanofluid 9(2):211–223
22. Sadeghi M, Sadeghi A, Saidi MH (2016) Electroosmotic flow in hydrophobic microchannels of general cross section. J Fluids Eng 138(3):031104
23. Silkina EF, Asmolov ES, Vinogradova OI (2019) Electroosmotic flow in hydrophobic nano-channels. Phys Chem Chem Phys 21(41):23036–23043
24. Rahmati AR, Khorasanizadeh H, Arabyarmohammadi MR (2019) Implementation of lattice Boltzmann method to study mixing reduction in isothermal electroosmotic pump with hydrophobic walls. J Transport Phenomena Nano-Micro Scales 7(1):28–36
25. Noreen S, Waheed S, Lu DC (2020) Influence of Joule heating and wall slip in electroosmotic flow via peristalsis: second law analysis. J Braz Soc Mech Sci Eng 42(6):295
26. Baños RD, Arcos JC, Bautista O, Méndez F, Merchán-Cruz EA (2021) Mass transport by an oscillatory electroosmotic flow of power-law fluids in hydrophobic slit microchannels. J Braz Soc Mech Sci Eng 43(9):1–15
27. Gao Y, Wong TN, Chai JC, Yang C, Ooi KT (2005) Numerical simulation of two fluid electroosmotic flow in microchannels. Int J Heat Mass Transf 48(25–26):5103–5111
28. Heghab HE, Liu G (2004) Fluid flow modeling of micro-orifieces using micropolar fluid theory. In: Microfluidics devices and systems III, vol 4177, pp 257–267
29. Dutta P, Beskok A (2001) Analytical solution of combined electroosmotic/pressure-driven flows in two dimentional straight channels finite Debye layer effects. Anal Chem 73(9):1979–1986
30. Ariman T, Cakmak AS (1968) Some basic viscous flows in micropolar fluids. Rheol Acta 7(3):236–242